

FSU-SCRI-96-13
GUTPA/96/2/8
OHSTPY-HEP-T-96-002
Edinburgh 96/1

B Spectroscopy from NRQCD with Dynamical Fermions

S. Collins

SCRI, Florida State University, Tallahassee, FL 32306-4052, USA
and Edinburgh University, Edinburgh, Scotland EH9 3JZ.

U. M. Heller and J. H. Sloan

SCRI, Florida State University, Tallahassee, FL 32306-4052, USA

J. Shigemitsu

The Ohio State University, Columbus, Ohio 43210, USA

A. Ali Khan¹ and C. T. H. Davies¹

University of Glasgow, Glasgow, Scotland G12 8QQ

Abstract

We present a lattice investigation, partially including the effects of dynamical quarks, of the heavy-light mesons using NRQCD for the heavy quark and the Wilson action for the light quark. We performed an extensive calculation of the spectrum employing a multi-state, multi-exponential fitting analysis which enabled us to extract the $2S-1S$ splitting as well as the $^1P_1-\bar{S}$ and hyperfine splittings. The Wilson action introduces a large systematic error into the calculation, and within this uncertainty we obtain agreement with experiment. We performed a comprehensive calculation of the heavy-light meson mass, investigating three methods and their range of validity. The agreement found between these methods confirms that Lorentz invariance can be restored at this order in NRQCD by a constant shift to all masses. We calculated spectroscopic quantities over a wide range in heavy quark mass and were able to perform a detailed investigation of heavy quark symmetry around the b quark mass. In particular, we extracted the nonperturbative coefficients of terms in the heavy quark expansion of the meson binding energy. We demonstrate the importance of using tadpole-improved operators in such a calculation.

PACS numbers: 12.38.Gc, 14.65.Fy, 14.40.Nd, 14.20.Mr

¹UKQCD Collaboration

1 Introduction

Lattice field theory has an important role to play in the study of B -Physics. Through this approach it is possible not only to perform a first principles calculation of experimentally important quantities, but also to test heavy quark symmetry predictions of Heavy Quark Effective Theory (HQET) and extract the nonperturbative coefficients of the heavy quark expansions which are required to extract numerical results from HQET. Furthermore, comparison with the predictions of various models for these coefficients provides a test of the underlying assumptions of the models.

The first stage of a lattice study of B mesons is the calculation of the spectrum. As the simplest quantity to extract, it is the foundation for more complicated calculations of B decay processes. A correct reproduction of the spectrum gives confidence in the calculational procedure, as well as providing predictions for states not yet measured experimentally. In the spectrum, several physical scales are important. The gross structure of the B spectrum is due to excitations of the light quark and hence mass splittings related to these, such as $P-S$ and $2S-1S$ are of $O(\Lambda_{QCD})$. Conversely, the heavy quark is approximately a static colour source and its spin affects the spectrum at the scale of the hyperfine splitting, $O(\Lambda_{QCD}^2/M)$.

Thus, to reproduce the spectrum, the systematic errors arising from both the heavy and light quarks must be rigorously controlled. Previously, simulating the b quark (as opposed to a static quark) on the lattice presented a major problem since the $O(Ma)$ discretisation errors of the standard relativistic fermionic action were $O(1)$ for a b quark on a typical lattice, $a^{-1} \sim 2.0$ GeV. However, the success of the non-relativistic QCD (NRQCD) approach in calculations of Υ spectroscopy [1, 2] shows that the b quark can be simulated directly on lattices currently available. In NRQCD the heavy quark mass scale is removed and the action becomes an expansion in the typical (non-relativistic) heavy quark velocity, which is a small parameter. The precision of the calculation is controlled simply by the order at which the expansion is truncated. For heavy-light mesons, the terms included in the action at each order in the heavy quark velocity is determined by the order of the terms in $1/M$; this is discussed in more detail in reference [3]. Considering the almost spectator role of the heavy quark in the heavy-light meson, we include only first order i.e. $O(1/M)$ terms in the NRQCD action in this study.

For light quarks, recent studies have shown [4, 5] that the $O(ma)$ discretisation errors of the Wilson action are significant for a high statistics calculation on typical lattices even for small bare masses (i.e. the constituent mass seems to be the important scale for $O(ma)$ effects). Improved light fermion actions, for example the tadpole-improved Clover action with errors of roughly $O(m^2 a^2)$, are needed. However, in this initial calculation we have employed the Wilson action and expect this to give rise to the dominant systematic error.

Another uncertainty in connecting lattice calculations to the physical world is the quenched approximation. In this study we have partially included the effects of dynamical quarks. In addition, these computations are performed in conjunction with a simulation using $\beta = 6.0$ quenched configurations [3] and in the future we expect to be able to isolate and remove the full effects of quenching.

The organisation of this paper is as follows. The details of the simulation are given in section 2 followed by a discussion of the expected systematic errors. Particular attention has been paid in our analysis to the fitting procedure and extraction of ground and excited state energies. Our methods are outlined in section 4 and illustrated with a subset of the data. We use the results over a range of heavy quark masses to investigate heavy quark symmetry in the meson binding energy in section 5.2. The lowest order coefficients of the heavy quark expansion $\bar{\Lambda}$ and $\langle -\bar{D}^2 \rangle$ are extracted. The heavy-light meson mass is calculated in section 5.2.1; three methods are compared and their range of validity investigated. In section 5.3 we turn to the mass splittings, B^*-B , $B^{**}-B$ and B_s-B , and compare the simulation results with experiment and the expectations of heavy quark symmetry. The conclusions and a summary of the spectrum are given in section 6.

2 Simulation Details

The simulations were performed using 100 $16^3 \times 32$ gauge configurations at $\beta = 5.6$ with two flavours of staggered dynamical sea quarks with a bare quark mass of $am_{sea} = 0.01$. These configurations were generously made available by the HEMCGC collaboration; more details can be found in [6]. We fixed the configurations to the Coulomb gauge. The light quark propagators were generated using the Wilson fermion action, without an $O(a)$ improvement term, at two values of the hopping parameter, $\kappa = 0.1585$ and 0.1600 . The former corresponds to a quark mass close to strange, where $\kappa_s = 0.1577$ from M_ϕ , while 0.1600 is somewhat lighter, with $\kappa_c = 0.1610$.

In this simulation we truncate the NRQCD series at $O(1/M_0)$ and the action takes the form:

$$S = Q^\dagger (D_t + H_0 + \delta H) Q \quad (1)$$

where

$$H_0 = -\frac{\Delta^{(2)}}{2M_0} \quad \text{and} \quad \delta H = -c_B \frac{\sigma \cdot B}{2M_0}. \quad (2)$$

Tadpole improvement of the gauge links is used throughout, where $u_0 = 0.876$ measured from the plaquette, and the hyperfine coefficient is given the tree-level value $c_B = 1$. We use the standard Clover-leaf operator for the B field. A constant mass term has been omitted from the action for simplicity of the calculation. It has no effect on mass splittings and amplitudes and a suitable energy shift for all masses can be added post-simulation. This will be discussed in further detail in

section 5.2.1. The heavy quark propagators were computed using the evolution equation:

$$\begin{aligned} G_1 &= \left(1 - \frac{aH_0}{2n}\right)^n U_4^\dagger \left(1 - \frac{aH_0}{2n}\right)^n \delta_{\vec{x},0} \\ G_{t+1} &= \left(1 - \frac{aH_0}{2n}\right)^n U_4^\dagger \left(1 - \frac{aH_0}{2n}\right)^n (1 - a\delta H)G_t \quad (t > 1) \end{aligned} \quad (3)$$

In the static limit this reduces to

$$G_{t+1} - U_4^\dagger G_t = \delta_{x,0} \quad (4)$$

The parameter n is introduced to stabilise unphysical higher momentum modes as M_0 is decreased and from perturbation theory one estimates $n \gtrsim 3/M_0$. This is only a rough guide and for a high statistics simulation a more conservative lower limit on n may be needed to ensure a smooth transition between regions of different n as M_0 decreases. This point will be illustrated in Section 5.1.

The heavy quark propagators were computed over a range of values of M_0 to probe both the lower limit of NRQCD where the perturbative couplings diverge and the theory breaks down, around $aM_0 \lesssim 0.6$ [7], and the $aM_0 \rightarrow \infty$ limit where *signal/noise* becomes poor as NRQCD tends to the static limit. Note that for heavy-light mesons there is no upper limit imposed on M_0 by discretisation errors in the heavy quark motion, $ap_Q \sim a\Lambda_{QCD} \sim 0.2 \ll 1$ independent of M_0 (where we take $a\Lambda_{QCD} = a\Lambda_V = 0.185$ for these configurations). This is in contrast to heavy-heavy mesons where the kinetic energy, not the momentum, of the heavy quark is approximately Λ_{QCD} and $ap_Q \sim \sqrt{a^2 M \Lambda_{QCD}}$. Thus, discretisation errors naively become large when $ap_Q \sim 1$ i.e. $aM \sim 1/a\Lambda_{QCD} \sim 5$. We generated heavy quark propagators at 11 values of (aM_0, n) corresponding to (0.8,5), (1.0,4), (1.2,3), (1.7,2), (2.0,2), (2.5,2), (3.0,2), (3.5,1), (4.0,1), (7.0,1) and (10.0,1), and the static limit. This roughly corresponds to a range of meson masses from $M_B/2$ to $4M_B$ and is sufficient for a reasonable investigation of heavy quark symmetry. However, it is not possible to simulate the D meson on this lattice using NRQCD; a larger lattice spacing is required, $\beta^{n_f=2} \lesssim 5.5$ or $\beta^{n_f=0} \lesssim 5.85$.

A NRQCD heavy quark propagator describes the forward propagation of a quark. To increase statistics we applied the time reversal transformation to both the gauge fields and the light quark propagators and repeated the heavy quark evolution; this is equivalent to calculating the propagation of the backwardly moving anti-particle.

Following the methods of [1, 8] meson correlation functions corresponding to both S and P states were constructed from the quark propagators using interpolating operators at the source of the form:

$$O = \sum_{\vec{x}_1, \vec{x}_2} Q^\dagger \Gamma^\dagger(\vec{x}_1 - \vec{x}_2) q(\vec{x}_2), \quad (5)$$

$^{2S+1}L_J (J^{PC})$	Ω
$^1S_0 (0^{-+})$	\hat{I}
$^3S_1 (1^{--})$	σ_i
$^1P_1 (1^{+-})$	Δ_i
$^3P_0 (0^{++})$	$\sum_j \Delta_j \sigma_j$
$^3P_1 (1^{++})$	$\Delta_i \sigma_j - \Delta_j \sigma_i$
$^3P_2 (2^{++})$	$\Delta_i \sigma_i - \Delta_j \sigma_j$
	$\Delta_i \sigma_j + \Delta_j \sigma_i$
	$(i \neq j)$

Table 1: The lattice operators, Ω , and associated quantum numbers used in the simulation. Ω is a 4×2 matrix in spin space. Note that since charge conjugation is not a good quantum number for the heavy-light system there is mixing between the 1P_1 and 3P_1 states.

and O^\dagger at the sink, where $\Gamma = \Omega\phi(\vec{x}_1 - \vec{x}_2)$ specifies the quantum numbers (Ω) of the state, detailed in table 1, and the smearing (ϕ) applied to the heavy quark. Smearing functions motivated by the hydrogen model were chosen to project out the ground and first excited state; for S-states

$$\begin{aligned}\phi_1(r) &= e^{-r/r_0} \\ \phi_2(r) &= (1 - r/(2r_0))e^{-r/(2r_0)}\end{aligned}\quad (6)$$

where $r_0 = 3.0$. Similarly for P-states

$$\begin{aligned}\phi_1(r) &= (-1 - r/(2r_0))e^{-r/(2r_0)} \\ \phi_2(r) &= (r/(3r_0))^2 e^{-r/(3r_0)}\end{aligned}\quad (7)$$

It is sufficient to use the same radius, r_0 , for all M_0 since the heavy quark is almost a spectator in the heavy-light system and the meson wavefunction is not expected to change significantly with M_0 . A delta function was also used for both S and P states.

With the aim of performing a multi-state, multi-correlation function analysis the heavy quark was smeared using all the source-sink combinations of the smearing functions. The meson propagator is then

$$C_{sc,sk}(\vec{p}, t) = \sum_{\vec{y}_1, \vec{y}_2} Tr \left[\gamma_5 (L^{-1})^\dagger(\vec{y}_2) \gamma_5 \Gamma^{(sk)\dagger}(\vec{y}_1 - \vec{y}_2) \tilde{G}_t(\vec{y}_1) \right] e^{-i\frac{\vec{p}}{2} \cdot (\vec{y}_1 + \vec{y}_2)} \quad (8)$$

where

$$\tilde{G}_t(\vec{y}_1) = \sum_{\vec{x}} G_t(\vec{y} - \vec{x}) \Gamma^{(sc)}(\vec{x}) e^{i\frac{\vec{p}}{2} \cdot \vec{x}}, \quad (9)$$

and $sc, sk = 1, 2, l$ corresponding to the ground state, first excited state and delta function smearing functions respectively. L^{-1} is the light quark propagator. Finite momentum 1S_0 correlators were generated for a subset of the data, $aM_0 = 0.8-4.0$, at $a|\vec{p}| = 1$ and $\sqrt{2}$ in units of $\frac{\pi}{16}$. To improve statistics, where appropriate, the correlators were averaged over different polarisations and different momentum directions.

3 Systematic Errors

There are systematic errors associated with both the heavy and the light quark in the heavy-light meson. The truncation of the NRQCD series at $O(1/M)$ introduces an absolute systematic error of $O(\Lambda_{QCD}(\Lambda_{QCD}/M)^2)$ associated with the heavy quark. This corresponds to a relative error of $O(\Lambda_{QCD}/M)$ in quantities of $O(\Lambda_{QCD}(\Lambda_{QCD}/M))$, naively estimated to be $O(v) \sim 10\%$, and an $O((\Lambda_{QCD}/M)^2) \sim 1\%$ error in quantities of $O(\Lambda_{QCD})$. The use of tree-level coefficients for the relativistic corrections will introduce errors of the form $O(\alpha_S \Lambda_{QCD}(\Lambda_{QCD}/M))$, which are of the same magnitude as those above for $\alpha_S \sim 0.1$. Similarly, the magnitude of the scaling violations due to using the Wilson action for the light quark are $O(\Lambda_{QCD}^2 a)$, or a relative error of $O(\Lambda_{QCD} a) \approx 20\%$ for this ensemble. Hence, the systematic errors associated with the light quark are expected to dominate and the finite volume errors for a lattice of size ≈ 1.6 fm are unlikely to be larger than this for a B meson. It is important to note that this is a high statistics calculation with statistical errors of around 5%, much smaller than the systematic errors.

An indication of the size of the light quark uncertainties in the simulation can be found by comparing the lattice spacing obtained from various quantities. Table 2 details the values of a^{-1} extracted from various light spectroscopic quantities for this ensemble, where the Wilson action was used for the light quarks. Also included is the inverse lattice spacing obtained from the Υ spectrum using NRQCD [1]. In this case all terms in the NRQCD series were included up to $O(Mv^4)$ and the estimated systematic error is $\sim 1\%$. Clearly there is marked lack of agreement in the values obtained from observables dominated by presumably similar typical physical scales indicating large light quark uncertainties. In addition there is disagreement between the scale obtained from light and heavy spectroscopy. With partial inclusion of quark loops at finite sea quark mass, the running of the strong coupling does not match that in the real world but should provide an improvement on the quenched approximation. At present the light quark uncertainties in the spectroscopy hide any indication of this and the variation in the lattice spacing is similar to that found for a lattice with a similar a^{-1} ($\beta \sim 6.0$) in the quenched approximation. Currently, the light quark spectroscopy is being re-analysed using a multi-smearing, multi-state analysis with Clover fermions [4].

A large uncertainty in a^{-1} translates into similar uncertainties in predictions for physical quantities. While it is useful to quantify these by using a range of values for a^{-1} to convert into physical units, observables will exhibit systematic errors differently and the resulting uncertainty may not necessarily be expressible by merely using a range of values for a^{-1} . With this caveat we will take $a^{-1} = 1.8 - 2.4$ GeV. The emphasis of our analysis will be on determining the heavy quark mass dependence of various quantities and the nonperturbative coefficients of the $O(1/M)$ terms.

With light quark propagators at only two values of κ_l and with a much worse signal to noise ratio for the data at $\kappa_l = 0.1600$ compared to $\kappa_l = 0.1585$, it is not possible to perform a trustworthy chiral extrapolation. In addition, the light quark uncertainties affect the determination of the bare strange quark mass. κ_s extracted from pseudoscalar mesons, using the lowest order chiral mass dependence to find the ‘experimental mass’ of the pure $s\bar{s}$ pseudoscalar, differs from κ_s obtained from the vector meson ϕ . Thus, most of the results presented will be for $\kappa_l = 0.1585$.

“force”	2055
m_ρ	2140
m_p	1800
$\Upsilon(\text{NRQCD})$	2400

Table 2: a^{-1} in MeV obtained from various observables for this ensemble. The “force” is calculated from the static quark potential using r_0 . Statistical errors are 50 – 100 MeV.

4 Analysis

With three smearing functions for the heavy quark in all source-sink combinations we generated a 3×3 matrix of meson propagators, $C_{ij}(t)$, for each state, where $i, j = 1, 2, l$. With several independent determinations of the meson correlation function it is possible to perform simultaneous multi-exponential fits and thus rigorously constrain the ground state energy and amplitudes of the meson; higher excited states can also be obtained. Using a subset of the data involving correlation functions smeared at the source and local at the sink, vector fits were performed using the fitting function,

$$C_{il}(t) = \sum_{n=1}^{n_{exp}} b(i, n) e^{-E_n t} \quad i = 1, 2 \quad (10)$$

where n_{exp} is the number of exponentials used in the fit. Similarly,

$$C_{ij}(t) = \sum_{n=1}^{n_{exp}} a(i, n)a(j, n)e^{-E_n t} \quad i, j = 1, 2. \quad (11)$$

was used to fit to the 2×2 matrix of correlators formed from the correlators smeared using the ground and first excited state smearing function.

The fitting procedure applied to extract the mass spectrum from these correlation functions can be expressed as follows:

1. Choose the end of the fitting range, t_{max} , to be a timeslice where the $noise/signal \gtrsim 3$.
2. Begin with a 1 exponential correlated fit.
3. Vary the beginning of the time range, t_{min} , over all possible values i.e. $n_{cor}(t_{max} - t_{min} + 1) - n_{par} > 0$, where n_{cor} is the number of correlation functions and n_{par} the number of parameters in the fit.
4. Accept fits for which the quality of fit parameter $Q > 0.1$.
5. In the case of multi-correlation function fits repeat (3) including 2 then 3 exponentials.

For each set of fits with a fixed number of exponentials, the criteria for the ‘best’ fit is taken to be the earliest value of t_{min} where Q has reached a plateau i.e. is stable to successive increases in t_{min} .

With each addition of another exponential to the fit function the range of t_{min} with an acceptable Q moves closer to the origin and the extra exponential removes the excited state contamination from the lower state. A plateau is sought in the ground state fit parameters obtained using 1, 2 and 3 exponential fits. To achieve this and resolve the first, and higher, excited states there must be a sufficiently different overlap with the ground and excited states between the correlation functions with different smearing combinations. In addition, a signal for isolating the first excited state must be a non-zero overlap of the state with the excited state smearing function. In general, the highest excited state is likely to be untrustworthy, i.e. a 3 exponential fit is needed to provide confidence in the first excited state.

In order to perform correlated fits to quantities as a function of the meson mass 100 bootstrap ensembles were generated for each correlated fit to the propagators. However, we found that our statistics were insufficient to be able to perform the bootstrap procedure above $n_{exp} = 1$. Thus, only $n_{exp} = 1$ fits were used. It was possible to do this with confidence only because we were able to check agreement with the multi-state, multi-smearing analysis of the unbooted correlation functions.

In the construction of the correlation functions we are combining light quark propagators which include the contribution of the backwardly propagating anti-quark with the NRQCD heavy quark propagating solely in the forward direction. This leads to a unphysical contribution to the meson correlation function which should be small at least through $t_{max} \approx L_t/2 = 16$. Examination of the correlation functions indicates the contribution is small for $t_{max} \lesssim 24$.

5 Results

5.1 Fitting results for E_{sim}

The simplest quantities to extract are the 1S_0 and 3S_1 energies, E_{sim}^{PS} and E_{sim}^V respectively, which determine the exponential fall-off of the S-state correlators. With the omission of the constant mass term in the NRQCD action E_{sim} is not the meson mass, M_2 ; the calculation of this quantity is discussed in the next section. However, physical mass splittings can be obtained from differences in E_{sim} for different mesons. In particular, to have confidence in the results it is vital to ensure the excited state contamination of E_{sim} is minimal. We use the $aM_0 = 1.0$ and $\kappa_l = 0.1585$ results to illustrate how we achieve this with our fitting analysis.

Figure 1 shows the effective masses of all the 1S_0 smeared correlation functions. The correlators smeared with the excited state smearing function have a larger contribution from excited states compared to those smeared only with the ground state smearing function, as required to separate ground state and excited states. Increasing M_0 from 1.0 to 10.0 corresponds to an approximate 7-fold increase in the meson mass. However, a comparison with the effective mass of C_{1l} for $aM_0 = 10.0$ in figure 7 shows there is only a gradual change in the meson wavefunction, as expected from a hydrogen-like picture where the heavy quark plays a minor role.

The 1S_0 ground state energy extracted from the $n_{exp} = 1, 2$ and 3 vector fits is presented in figure 2 as a function of t_{min} , with t_{max} fixed at 20. Fits are shown for which $Q > 0.1$ and for which all states included in the fit are resolved. For example the $n_{exp} = 2$ vector fit provides results for E_{sim} consistent with $n_{exp} = 1$ for $t_{min} > 10$. The first excited state, however, is no longer resolved as seen by an excited state amplitude consistent with zero. A $n_{exp} = 3$ fit can be performed using $t_{min} = 2$ and 1. This does not give sufficient additional timeslices, however, to resolve the third excited state.

A noticeable feature is the 2σ ‘wobble’ in E_{sim} which also appears in the effective mass of the $C_{1l}(t)$ correlator. There are two possibilities, excited state contamination or finite statistics. If the former is responsible the contribution from excited states is small enough that it cannot be resolved using $n_{exp} = 2$. Thus, we quote the uncertainty in E_{sim} due to the fitting procedure to be 2σ .

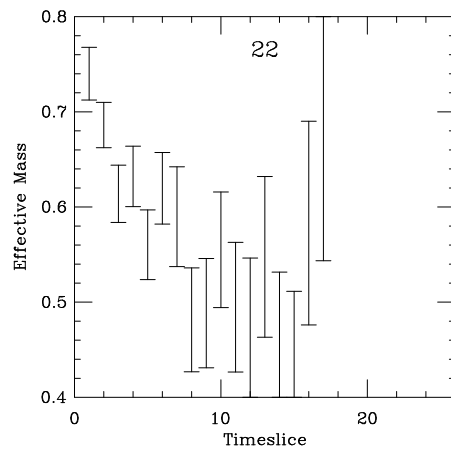
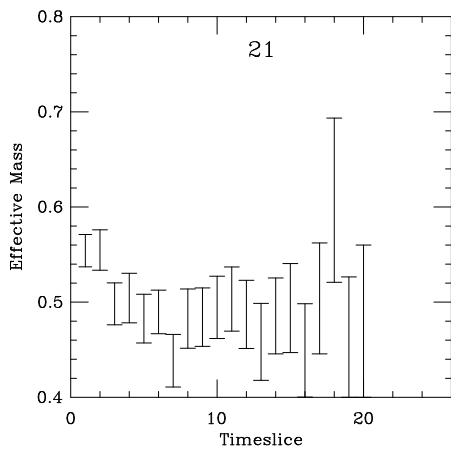
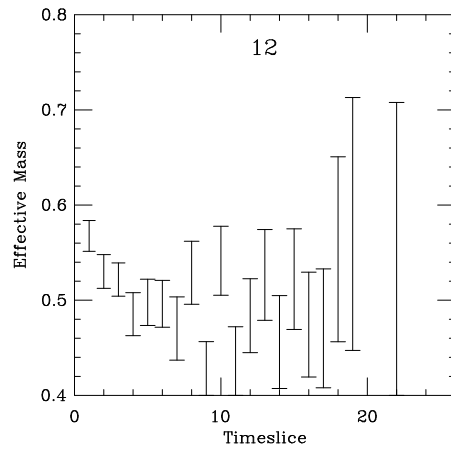
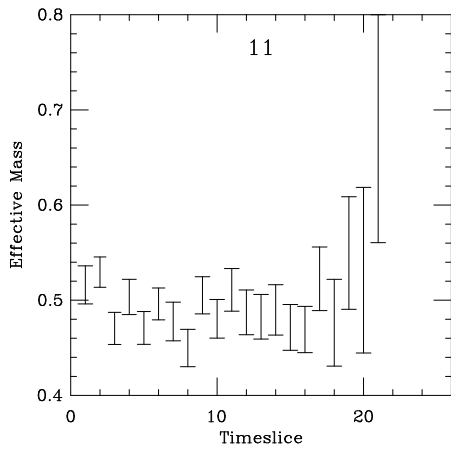
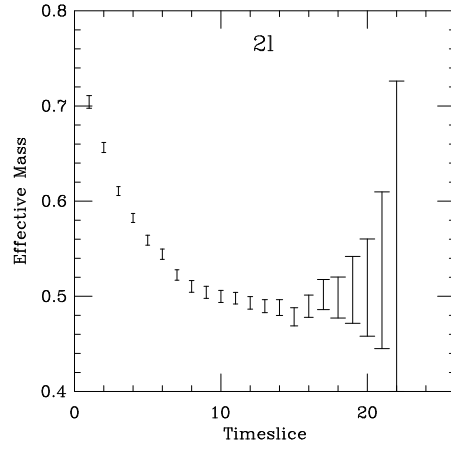
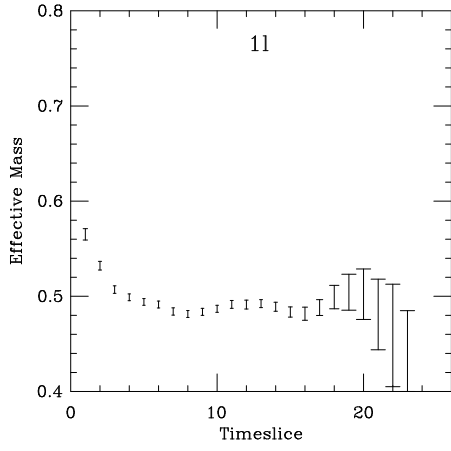


Figure 1: The effective masses of the 1S_0 meson correlators for $aM_0 = 1.0$ and $\kappa_l = 0.1585$.

Data	n_{exp}	fit range	Q	aE_{sim}	aE'_{sim}
11,21	2	3-20	0.2	0.484(2)	0.83(2)
11,12,21,22	2	3-16	0.8	0.485(2)	0.80(2)
11	1	3-20	0.9	0.485(3)	-

Table 3: A comparison of the energies extracted from fits to 3 data sets of 1S_0 correlators for $aM_0 = 1.0$ and $\kappa_l = 0.1585$

This feature is seen in the results for all values of M_0 .

We found E'_{sim} for the first excited state extracted using $n_{exp} = 2$ to be stable around 0.8 and the corresponding amplitude to be well determined for $t_{min} = 2-6$; in this region there is a significant excited state contribution to C_{2l} while the ground state dominates C_{1l} . A $n_{exp} = 3$ fit over a wider range in t_{min} is needed to provide confidence in this result. C_{ll} was not found to be useful in providing a larger overlap with the first or second excited state since even higher excited states were also present with significant contributions.

A similar picture is found in the results for the matrix fits presented in figure 3. E_{sim} and E'_{sim} are consistent as t_{min} and n_{exp} are varied and in agreement with those obtained using the vector fit. This is proof that we have isolated the ground state and minimised excited state contributions to E_{sim} .

As mentioned previously, we were limited to bootstrapping only $n_{exp} = 1$ fits. So we also performed $n_{exp} = 1$ correlated fits to the $C_{11}(t)$ correlation functions. The effective mass and values of E_{sim} obtained, with the corresponding values of Q , are shown in figure 4. A plateau can be seen in the variation of E_{sim} with t_{min} from $t_{min} = 3$. Table 3 compares the best fits from all three fitting methods. The values for the ground state using multi-exponential fits are consistent with the $n_{exp} = 1$ fit to $C_{11}(t)$. The statistical error in the fits to C_{11} is larger. However, this will not affect quantitative results of the analysis as the systematic errors are much larger than the statistical errors.

The fitting range of 3–20 was found to be optimal for the 1S_0 state for all M_0 at $\kappa_l = 0.1585$, while for 3S_1 , 4–20 was used. Table 4 details the corresponding values of E_{sim}^{PS} and E_{sim}^V . The first excited state energy extracted using $n_{exp} = 2$ correlated fits to the vector of smearing functions with the fitting range 3–20 for $aM_0 = 1.0, 2.0$ and 4.0 are presented in table 5. The $E'_{sim} - E_{sim}$ splitting is of the order of $a\Lambda_{QCD} \sim 0.2$, and only weakly dependent on the heavy quark mass, as expected for the excitation of a light quark within the heavy-light meson.

We were not able to perform such an extensive analysis in the static limit. Figure 5 presents the effective masses for the C_{1l} , C_{2l} and C_{11} correlation functions for a static heavy quark and $\kappa_l = 0.1585$. The static results suffer from the signal disappearing around timeslice 11. The smeared correlators C_{12} , C_{21} and C_{22} are dominated by noise and are not useful. We performed $n_{exp} = 1$ correlated fits to

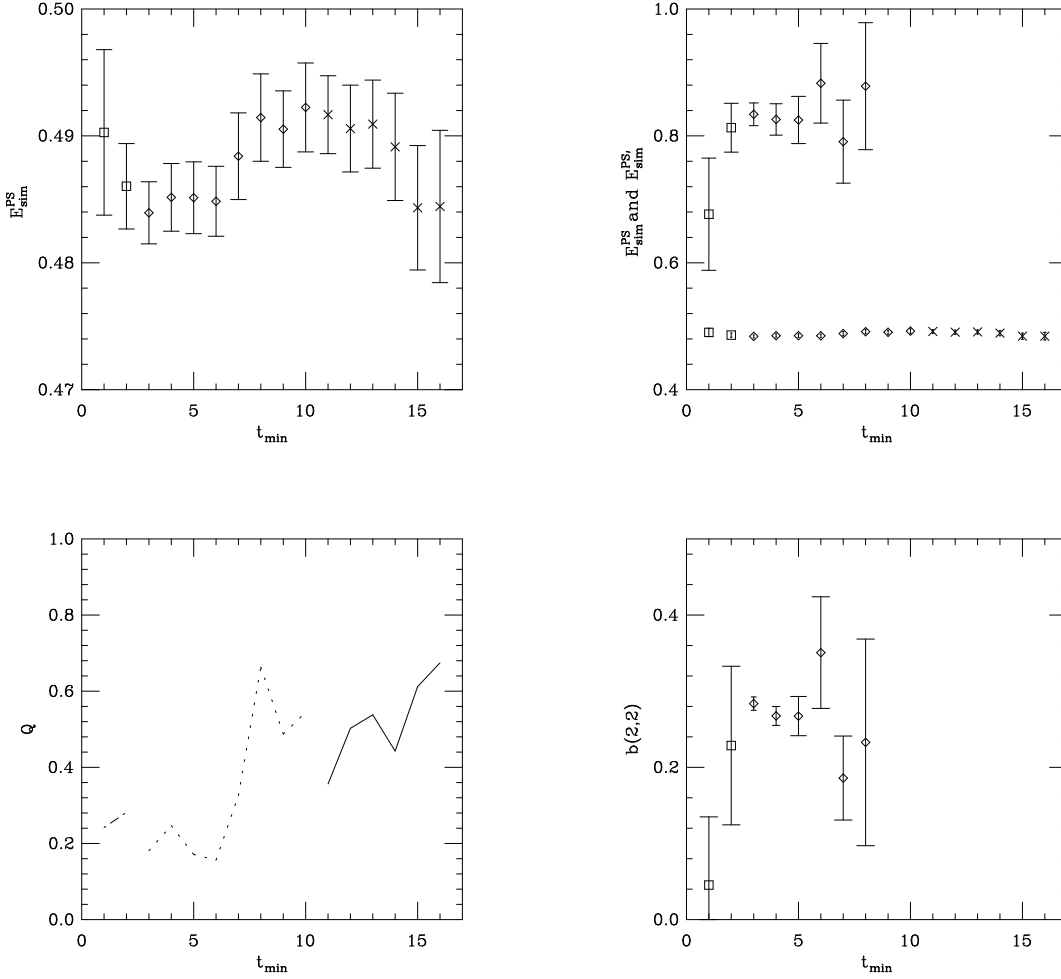


Figure 2: The variation of 1S_0 ground and first excited state energies with t_{min} extracted from vector fits to the C_{1l} and C_{2l} meson correlators for $aM_0 = 1.0$ and $\kappa_l = 0.1585$. Fits performed with $n_{exp} = 3$ are shown as squares, diamonds represent $n_{exp} = 2$ and crosses $n_{exp} = 1$. Only fits for which $Q > 0.1$ are shown. The variation of Q with t_{min} is shown as the solid line for $n_{exp} = 1$ fits, the dotted line for $n_{exp} = 2$ and the dashed line for $n_{exp} = 3$. t_{max} is fixed at 20. Also presented is $b(2,2)$, the overlap of the first excited state with the C_{2l} correlator.

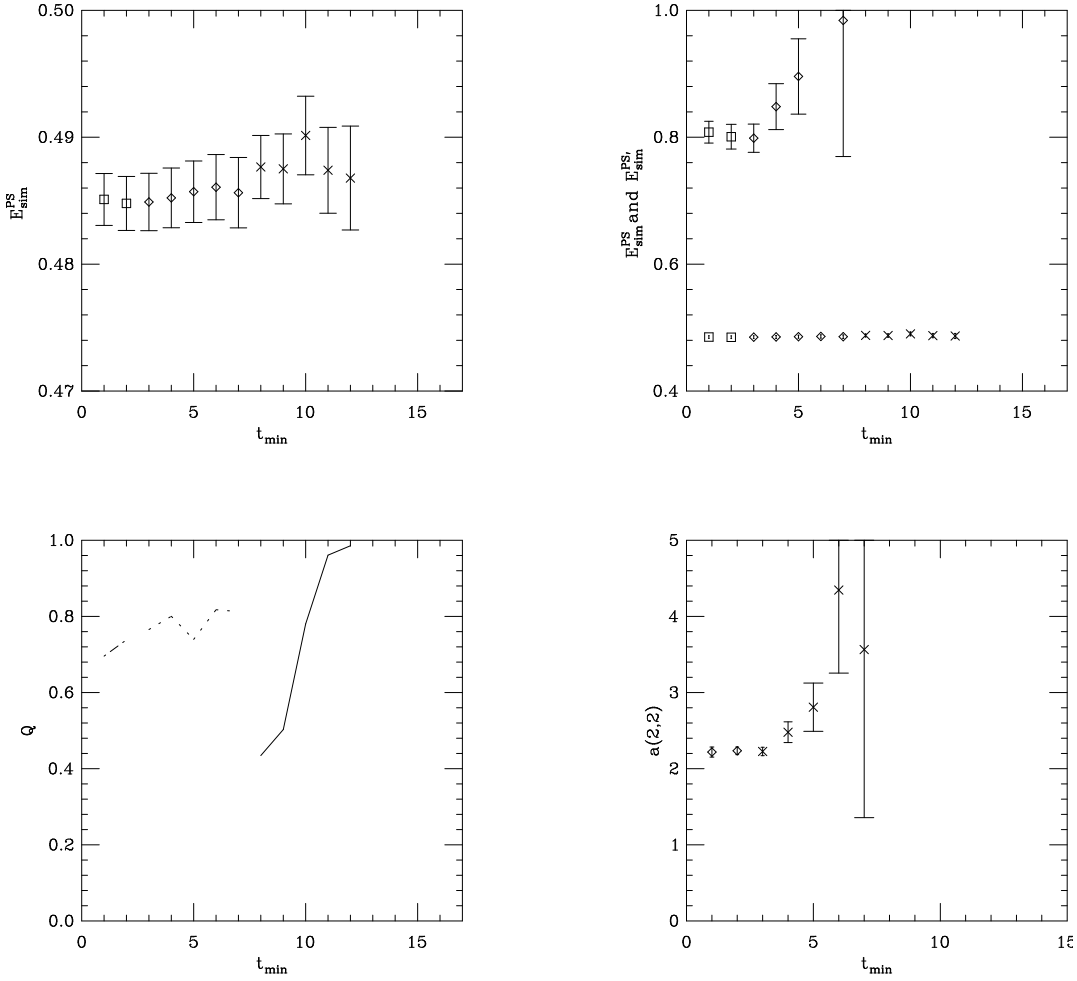


Figure 3: The variation of 1S_0 ground and first excited state energies with t_{\min} extracted from matrix fits to the C_{11} , C_{12} , C_{21} and C_{22} meson correlators for $aM_0 = 1.0$ and $\kappa_l = 0.1585$, where $t_{\max} = 16$. The same symbols are used as in the previous figure. Also presented is the overlap $a(2,2)$ of the first excited state with the excited state smearing function.

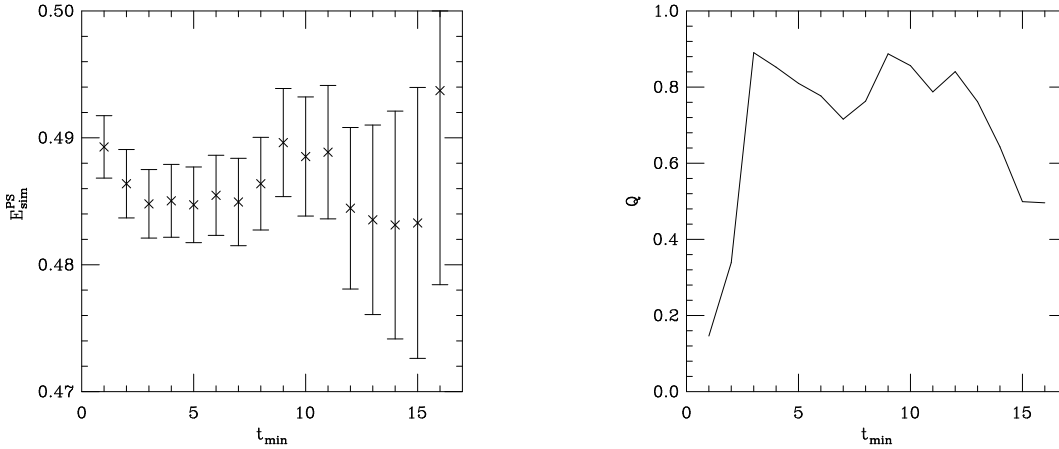


Figure 4: The variation of E_{sim}^{PS} with t_{min} extracted from a single exponential fit to C_{11} for $aM_0 = 1.0$ and $\kappa_l = 0.1585$, where $t_{max} = 20$.

aM_0	aE_{sim}^{PS}	aE_{sim}^V	$aE_{sim}^V - aE_{sim}^{PS}$
0.8	0.472(3)	0.502(3)	0.030(1)
1.0	0.485(3)	0.512(4)	0.026(2)
1.2	0.494(3)	0.517(4)	0.023(2)
1.7	0.506(3)	0.525(4)	0.018(2)
2.0	0.510(3)	0.527(4)	0.016(1)
2.5	0.514(4)	0.528(4)	0.014(1)
3.0	0.517(4)	0.529(4)	0.012(1)
3.5	0.519(4)	0.530(4)	0.010(1)
4.0	0.520(4)	0.530(4)	0.009(1)
7.0	0.522(4)	0.529(5)	0.007(1)
10.0	0.522(4)	0.528(5)	0.005(1)
∞	0.529(6)		-

Table 4: Ground state energies extracted from $n_{exp} = 1$ fits to C_{11} for $\kappa_l = 0.1585$. Also shown are the hyperfine splittings obtained from performing a single exponential fit to the ratio of the 3S_1 and 1S_0 C_{1l} correlators.

aM_0	aE_{sim}^{PS}	$aE_{sim}^{PS'}$	$a(2S-1S)$
1.0	0.485(3)	0.83(2)	0.34(2)
2.0	0.510(3)	0.81(2)	0.30(2)
4.0	0.520(4)	0.77(1)	0.25(1)

Table 5: Ground and first excited state 1S_0 energies obtained from $n_{exp} = 2$ fits to C_{1l} and C_{2l} for $\kappa_l = 0.1585$. Also shown is the splitting between the ground and first excited 1S_0 state.

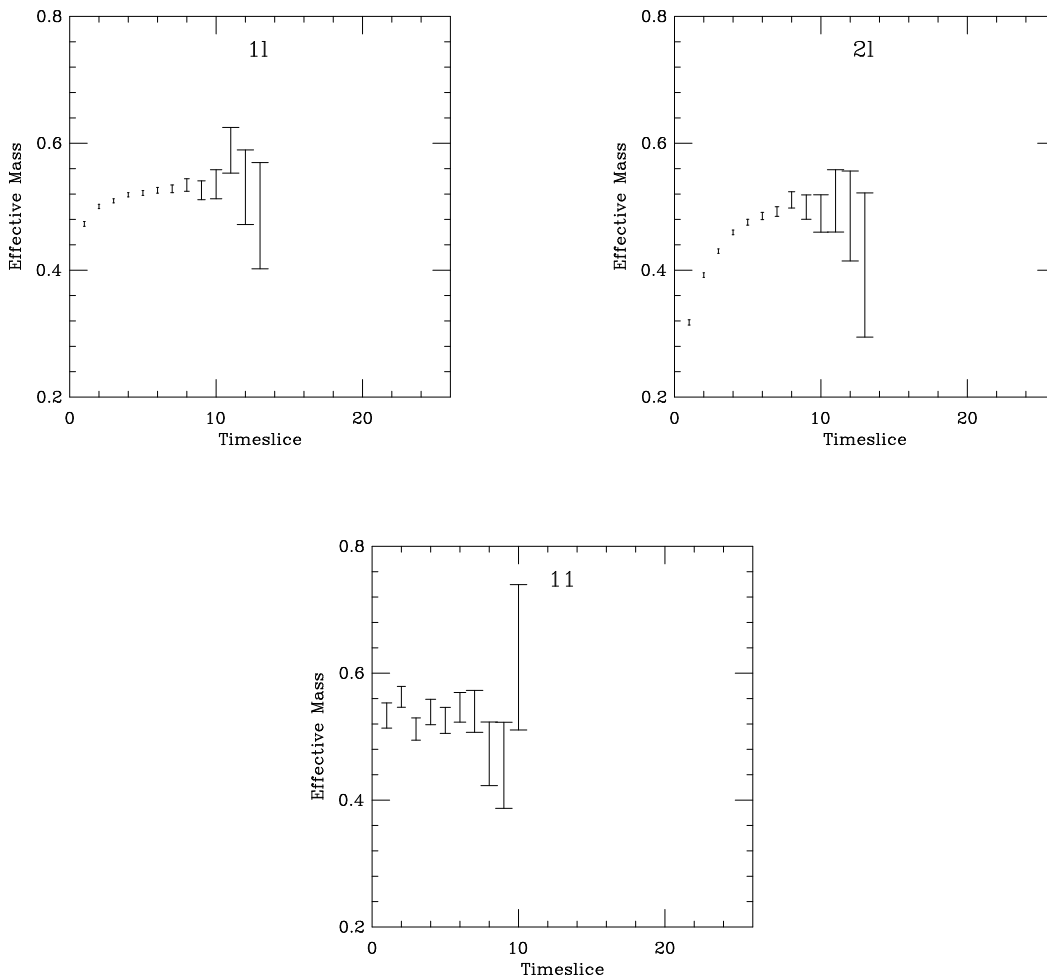


Figure 5: The effective masses of the 1S_0 meson correlators for $aM_0 = \infty$ and $\kappa_l = 0.1585$.

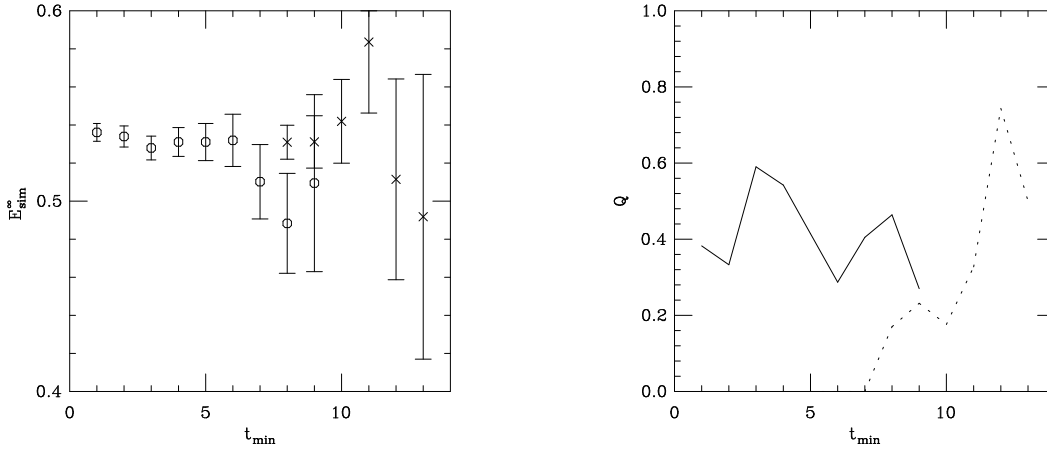


Figure 6: Single exponential fits to the 1S_0 C_{11} meson correlator (circles) and simultaneously to the C_{1l} and C_{2l} correlators (crosses) for $aM_0 = \infty$ and $\kappa_l = 0.1585$. $t_{max} = 11$ for the fits to C_{11} , and 15 for the fits to C_{1l} and C_{2l} . The corresponding values of Q are shown as a solid line for the fits to C_{11} and as a dotted line for the fits to C_{1l} and C_{2l} .

C_{11} and simultaneously to C_{1l} and C_{2l} , detailed in figure 6. A $n_{exp} = 2$ correlated fit to the vector of smeared correlators with $Q > 0.1$ was not found. The ground state and first excited state smearing functions are not sufficiently different with these statistics at early timeslices to resolve the first excited state. Consistency is found between the vector fits and the single exponential fits to C_{11} and we choose the latter with the time range 3–11 as the best fit.

The static case is the infinite quark mass limit of NRQCD. Thus, in the smooth transition from finite M_0 to the static limit the *signal/noise* problems, associated with $aM_0 = \infty$, will also present a problem at finite M_0 when the heavy quark mass is large enough. However, as seen in figure 7 we found that even the highest value of M_0 used is not hampered by noise and the signal for the ground state remained out to timeslices of 18-20. The static limit appears to be a special point with poor *signal/noise* properties and our conclusions about the static result will actually rely on the infinite mass extrapolation of the more accurate NRQCD results.

5.2 Variation of E_{sim} with heavy quark mass

The results for E_{sim} for both 1S_0 and 3S_1 at finite M_0 and in the static limit are plotted against $1/M_0$ in figure 8. As M_0 increases and the hyperfine interaction becomes smaller the S-states become degenerate and tend towards the static result where flavour and spin symmetry are restored. This agreement with the static result coupled with the multi-state, multi-smearing analysis at finite M_0

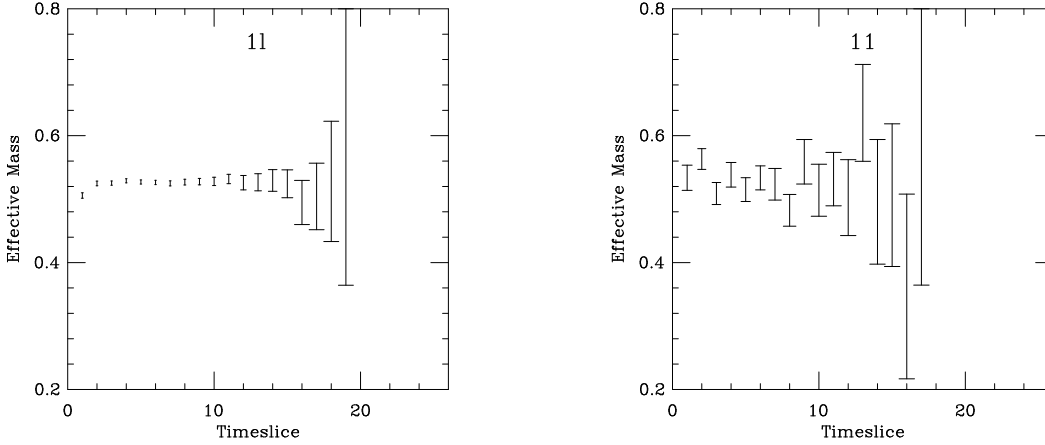


Figure 7: The effective masses of the 1S_0 meson correlators for $aM_0 = 10.0$ and $\kappa_l = 0.1585$.

suggests that the excited state contribution to E_{sim} for $aM_0 = \infty$ is small. In addition, the deviation from the static limit around the B meson ($aM_0 \sim 2.0$ see Section 5.2.1) is small and of order a few percent as expected by naive power counting arguments.

In the same way as for the NRQCD action, E_{sim} and other meson quantities can be parameterised in the heavy quark limit in terms of an expansion in $1/M$. The coefficients of the expansion are nonperturbative quantities which can be extracted from the simulation. From first order perturbation theory in $(H_0 + \delta H)$ about the static limit we obtain

$$E_{sim} = E_{sim}^\infty + \infty \langle P | \bar{Q} (-\vec{D}^2 - c_B \sigma \cdot B) Q | P \rangle^\infty \frac{1}{2M_0} + O\left(\frac{1}{M_0^2}\right). \quad (12)$$

where $|P\rangle^\infty$ represents the meson in the limit of infinite heavy quark mass and the $O(1/M_0)$ coefficient is merely the expectation value of the kinetic and hyperfine terms appearing in the NRQCD action. Note that the possibility of using a different choice of expansion parameter in equation 12 introduces an $O(1/M_0)$ uncertainty in the first order coefficient. E_{sim}^∞ is related to the binding energy of the heavy-light meson, $\bar{\Lambda}$, in the static limit:

$$\bar{\Lambda} = \lim_{m_Q \rightarrow \infty} (M_{hl} - m_Q) \quad (13)$$

$$= E_{sim}^\infty - E_0^\infty \quad (14)$$

where m_Q is the pole mass and E_0^∞ is the energy of a heavy quark in the static theory. Both $\bar{\Lambda}$ and $\infty \langle P | \bar{Q} (-\vec{D}^2 - c_B \sigma \cdot B) Q | P \rangle^\infty$ appear in expressions for $O(1/M)$ corrections to HQET predictions, but cannot be calculated using HQET alone.

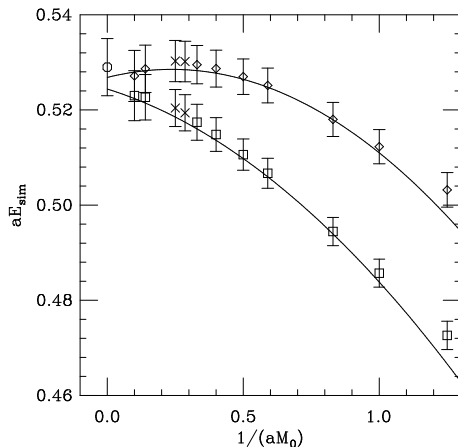


Figure 8: aE_{sim} vs $1/(aM_0)$ for 1S_0 (squares) and 3S_1 (diamonds) for $\kappa_l = 0.1585$. The static value is shown as a circle and the solid lines show quadratic fits to the heaviest six data points. The data points shown as crosses correspond to $aM_0 = 3.5$ and 4.0 and are not included in the fits.

To extract these quantities we performed correlated fits to the data as a function of $1/M_0$ using the functional form

$$E_{sim} = C_0 + \frac{C_1}{M_0} + \frac{C_2}{M_0^2} + \frac{C_3}{M_0^3}. \quad (15)$$

The fitting procedure was similar to that for the propagator fits; beginning with a constant fit function the endpoint for the fit is fixed to the heaviest data point, $aM_0 = 10.0$, and the initial point is varied over all finite values of M_0 . The procedure is repeated for a linear, quadratic and a cubic fit. The results for the 1S_0 meson are shown in table 6, where, except for the fits to a constant, only ‘good’ fits to the data are presented (defined as $Q > 0.1$).

The variation of the data with $1/M_0$ is consistent with a constant only for the heaviest two data points, while a linear term is required in the region of the B_s meson and a quadratic term for $1/aM_0 \gtrsim 0.8$. The lightest two points require a fit function of higher order than a cubic function to be included in a fit. Since we have truncated the NRQCD action at $O(1/M_0)$ the coefficients of the quadratic term are not correct and if the results are to connect with simulations around the D meson the $O(1/M_0^2)$ terms in the action are needed.

In general, in order to obtain stable values for C_i the fit must include C_{i+1} . The results for C_0 from both the linear and quadratic fits are consistent, and also in agreement with the static result. There are not sufficient data points in the quadratic region to determine whether the value for C_1 is stable around ~ -0.03 . Hence, only a rough determination of the coefficients is possible and the results are detailed in table 7 for both 3S_1 and 1S_0 . Quadratic fits to both E_{sim}^{PS} and E_{sim}^V

order	fit range	n.d.o.f	Q	aC_0	a^2C_1	a^3C_2
0	1-2	1	0.81	0.522(3)	-	-
	1-3	2	0.04	0.515(3)	-	-
1	1-3	1	0.55	0.527(4)	-0.029(8)	-
	1-4	2	0.61	0.529(4)	-0.036(5)	-
	1-5	3	0.29	0.533(3)	-0.044(3)	-
	1-6	4	0.44	0.532(3)	-0.043(2)	-
2	1-6	3	0.42	0.528(4)	-0.031(9)	-0.018(7)
	1-7	4	0.32	0.524(4)	-0.018(6)	-0.015(4)

Table 6: Correlated fits to E_{sim}^{PS} as a function of $1/M_0$ for $\kappa_l = 0.1585$. The fit range 1–3 denotes a fit to E_{sim}^{PS} at $aM_0 = 10.0, 7.0$ and 3.0 . The points at $aM_0 = 4.0$ and 3.5 are not included in the fits for reasons explained later.

	aC_0	a^2C_1
E_{sim}^{PS}	0.528(5)	-0.03(1)
E_{sim}^V	0.528(5)	-0.01(1)
\bar{E}_{sim}	0.530(5)	-0.02(1)

Table 7: The coefficients extracted from fits to E_{sim} as a function of $1/M_0$ for $\kappa_l = 0.1585$. The errors include the variation in the coefficients obtained using different orders in the fit function.

are shown in figure 8. The spin-average of the energies, $\bar{E}_{sim} = \frac{1}{4}(E_{sim}^{PS} + 3E_{sim}^V)$, removes the spin dependence and the slope of \bar{E}_{sim} depends only on the kinetic energy of the heavy quark. The results for \bar{E}_{sim} are also given in table 7.

It is useful to compare with previous results for the slope and intercept of E_{sim} . However, most other calculations have been performed in the quenched approximation; it is more appropriate to compare our results at $\beta^{n_f=0} = 6.0$ (using the tree-level Clover action for the light quarks as detailed in reference [3]) with those of other groups. In particular, Hashimoto [9] using NRQCD for the heavy quark and the Wilson action for the light quarks and Crisafulli et al [10] using the static approximation and the tree-level Clover action have results at this β value. Note that both groups use naive operators i.e. do not use tadpole improvement. In addition, taking into account the different systematic errors inherent in each of the simulations only a fairly rough comparison can be made.

Considering the intercept initially,

$$aE_{sim}^\infty = 0.60^1 \quad \text{Hashimoto} \quad (16)$$

$$= 0.61(1) \quad \text{APE Collaboration [11]}^2 \quad (17)$$

where $\kappa_l = \kappa_c$. This is in good agreement with our results at the same β value of $aE_{sim}^\infty = 0.461(15)$ taking into account the difference of $\ln u_0 = -0.13$ (where $u_0 = 0.878$ measured from the plaquette) since we use tadpole improved operators.

In order to calculate $\bar{\Lambda}$ from this quantity we use the tadpole-improved perturbative value of $E_0^\infty = 0.29(8)$ at $\beta^{n_f=0} = 6.0$ [7, 8]. E_0^∞ is an $O(\alpha_s)$ quantity and the corresponding error from omitting 2-loop corrections may be large, dominating the error in $\bar{\Lambda}$. Here the error in E_0^∞ is estimated by assuming the 2-loop corrections are roughly the square of the first order terms. Crisafulli et al suggest that as a linearly divergent quantity, nonperturbative effects may make a significant contribution to E_0^∞ and using a perturbative value will give rise to an ambiguity in the corresponding value for $\bar{\Lambda}$. Using a nonperturbative renormalisation procedure which aims to remove all mixing with lower dimensional operators they obtain the naive (non-tadpole improved) $E_0^\infty = 0.521(6)(10)$ [10]. However, the disagreement with the corresponding naive perturbative result, $E_0^\infty = 0.29(8) - \ln u_0 = 0.42(8)$, is only at the 1σ level. In addition, the nonperturbative result appears to be gauge dependent [12].

From equation 14 we obtain,

$$a\bar{\Lambda} = 0.17(10) \quad \kappa = \kappa_c \quad \beta^{n_f=0} = 6.0. \quad (18)$$

for our quenched results. The error is large enough to provide consistency with $a\bar{\Lambda} = 0.09(1)$ from Crisafulli et al.

For this study we find,

$$\begin{aligned} a\bar{\Lambda} &= 0.17(14) & \kappa &= 0.1585, \\ &= 0.13(14) & \kappa &= \kappa_c. \end{aligned} \quad (19)$$

using $E_0^\infty = 0.36(13)$ from perturbation theory. The results for the meson binding energy at finite values of M_0 , $\bar{\Lambda}_{M_0} \equiv E_{sim} - E_0$, are given in table 8 and will be referred to below. It is clear that the uncertainty in the perturbative value for E_0 must be reduced before a meaningful determination of the meson binding energy is possible with this approach.

Consider the slope of \bar{E}_{sim} with M_0 : in reference [3] we found results for C_1 similar to those presented in table 7,

$$a^2 C_1 = a^2 \langle -\vec{D}^2/2 \rangle_{bare}^{tadpole-improved} = -0.02(1) \quad \beta^{n_f=0} = 6.0 \quad (20)$$

independent of κ_l . The slope is small and negative. The naive, bare kinetic energy operator, however, is positive definite; in mean-field theory the two matrix elements are related by

$$\langle -\vec{D}^2/2 \rangle_{bare}^{tadpole-improved} = \langle -\vec{D}^2/2 \rangle_{bare}^{naive} - 3(1 - u_0). \quad (21)$$

¹The error in this quantity is not given.

²Crisafulli et al use the APE results generated on the same configurations for this quantity.

aM_0	3.0	3.5	4.0	7.0	10.0	∞
$\kappa_l = 0.1585$	0.168	0.171	0.174	0.172	0.171	0.172
$\kappa_l = \kappa_c$	0.129	0.133	0.135	0.132	0.134	0.131

Table 8: $a\bar{\Lambda}_{M_0}$ for the heavier quark mass values. The corresponding errors are of the same magnitude as those in equation 19.

Thus, we obtain an estimate for $a^2 \langle -\vec{D}^2/2 \rangle_{bare}^{naive} \sim +0.35$. Hashimoto extracted the slope of \bar{E}_{sim} (the hyperfine term is omitted from the NRQCD action), at $\kappa = \kappa_c$, and found $a^2 \langle -\vec{D}^2/2 \rangle_{bare}^{naive} = +0.33$ in good agreement with our results. Furthermore, Crisafulli et al, using their nonperturbative procedure calculate the matrix element explicitly and find $a^2 \langle -\vec{D}^2/2 \rangle_{bare}^{naive} = +0.36(7)$ for κ_l around κ_s . The overall agreement between different groups is encouraging. However, the dominance of the tadpole contributions to $\langle -\vec{D}^2/2 \rangle_{bare}^{naive}$ suggest it is better to quote the tadpole-improved matrix elements.

The physical kinetic energy of the heavy quark within the B meson, $\langle -\vec{D}^2 \rangle_{renorm}$, is a positive definite quantity and expected to be very small, of size $O(a^2 \Lambda_{QCD}^2) \sim 0.04$. The renormalised matrix element corresponds to the slope of $\bar{\Lambda}_{M_0}$ with respect to M_0 . From table 11, E_0 has a negative slope with M_0 and is of a magnitude that indicates a positive result for $\langle -\vec{D}^2 \rangle_{renorm}$ that is not inconsistent with $O(\Lambda_{QCD}^2)$. However, due to the large perturbative error our results for $\bar{\Lambda}_{M_0}$, shown in table 8, are consistent with a zero slope.

Also shown in figure 8 are the results for E_{sim}^{PS} and E_{sim}^V at $aM_0 = 3.5$ and 4.0. The stabilising parameter, $n = 1$, was used for both these values of M_0 . While this value satisfies $n \gtrsim 3/M_0$ the results for E_{sim} do not smoothly interpolate between the heavier data points with $n = 1$ and the lighter points which use $n = 2$. In particular, it was not possible to perform a correlated fit (even including higher powers in $1/M_0$ in the fit function) that includes $aM_0 = 3.5$ and 4.0 and the data at $aM_0 = 3.0, 2.5, \dots$ for which $n = 2$. The problem is remedied by increasing n for these values of aM_0 to 2 [13]; the shift in E_{sim} is much less than 1σ in the statistical errors and it is only the high correlations between results at different M_0 and our statistical accuracy that allows us to see this problem. Using $n = 1$ is sufficient for the heaviest data points at $aM_0 = 7.0$ and 10.0 and a correlated fit to the data can be performed omitting $aM_0 = 3.5$ and 4.0. These data points are omitted from all further fits to quantities as a function of $1/M$.

5.2.1 Meson Mass

The heavy-light meson mass, M_2 , can be calculated both perturbatively and nonperturbatively. It is important to find consistency between methods and investigate their range of validity, not least to confirm that Lorentz invariance

can be restored at this order through a mass shift to the heavy quark. We calculated M_2 in three ways:

1. Directly, from the dispersion relation. M_2 is the mass which appears in the kinetic term of a non-relativistic meson,

$$E(\vec{p}) = M_1 + \frac{|\vec{p}|^2}{2M_2} + \dots, \quad (22)$$

where $M_1 = E_{sim}$. For comparison with later results we define the heavy quark mass shift as $\Delta_{hl} = M_2 - M_1$. We extract $\Delta E = E(\vec{p}) - M_1$ by fitting the ratio of finite momentum to zero momentum 1S_0 correlators for C_{1l} and C_{2l} simultaneously to multiple exponentials for $|\vec{p}| = 1$ and $\sqrt{2}$ (for a fit involving more than one exponential this is not quite the right ansatz; however, it should allow most of our excited state contamination to be removed from ΔE). The next order term in the dispersion relation, $|\vec{p}|^4/8M_3^3$, is not correctly reproduced by our $O(1/M_0)$ action and thus $M_3 \neq M_2$. However, for lighter meson masses this term may be significant and we solve for M_2 using

$$\Delta E = \frac{|\vec{p}|^2}{2M_2} - \frac{|\vec{p}|^4}{8M_2^3}, \quad (23)$$

assuming $M_2 - M_3$ is small. Errors on the meson mass are obtained simply by solving for M_2 using $\Delta E \pm 1\sigma$.

As an example the results for 1S_0 at $aM_0 = 1.0$ and $\kappa_l = 0.1585$ for $|\vec{p}| = 1$ are shown in figure 9. The effective mass illustrates a difficulty in extracting M_2 from the dispersion relation; the smearing functions which are adequate for zero momentum have a reduced overlap with the ground state at finite momentum [14]. The effective mass does not plateau for $C_{1l}(|\vec{p}| = 1)/C_{1l}(|\vec{p}| = 0)$ until $t \approx 12$ (compared to $t \approx 5$ at zero-momentum), when the statistical errors are much larger than at earlier timeslices. However, the onset of the plateau is clear from a comparison of the effective mass using the excited state smeared source, which has a very different overlap with the ground and excited states. The variation of ΔE with t_{min} is stable from around $t_{min} = 13$ for $n_{exp} = 1$ and consistency is found with the results obtained with additional exponentials. A fitting range of 5–20 with $n_{exp} = 2$ is chosen for $aM_0 = 0.8$ to 2.0 and 13–20 with $n_{exp} = 1$ for $aM_0 = 2.5$ to 4.0; the corresponding values of ΔE are given in table 9. Finite momentum correlators were not generated for $aM_0 = 7.0$ and 10.0.

As the heavy quark mass increases, ΔE decreases, and correspondingly the determination of M_2 is statistically more uncertain. Table 10 details the results for M_2 from both $|\vec{p}| = 1$ and $\sqrt{2}$. Agreement between the meson

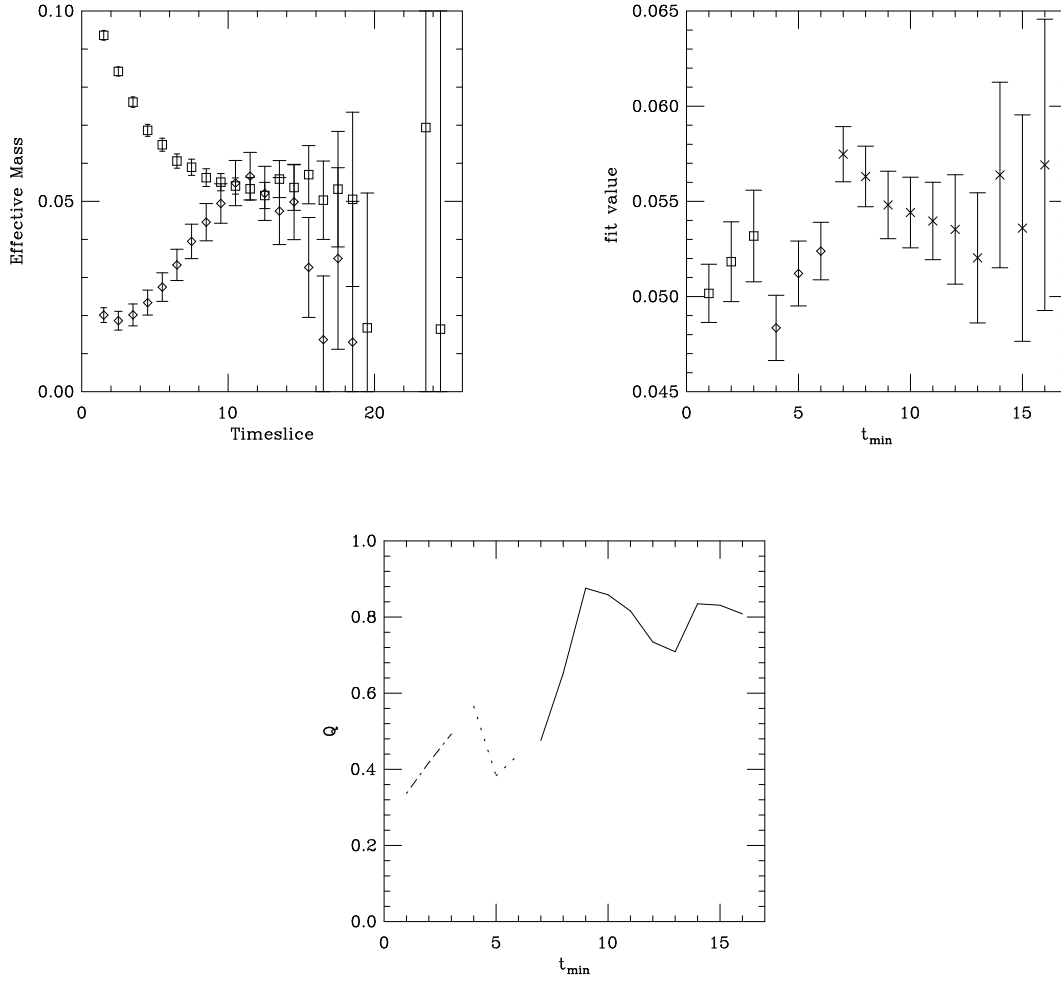


Figure 9: The effective masses of $C_{1l}(|\vec{p}| = 1)/C_{1l}(|\vec{p}| = 0)$ (squares) and $C_{2l}(|\vec{p}| = 1)/C_{2l}(|\vec{p}| = 0)$ (diamonds) for 1S_0 at $aM_0 = 1.0$ and $\kappa_l = 0.1585$. The fit parameter $\Delta E(\vec{p})$ extracted from 1 (crosses), 2 (diamonds) and 3 (squares) simultaneous exponential fits and the corresponding values of Q are also shown. t_{max} is fixed to 20.

aM_0	n_{exp}	fit range	Q	$a\Delta E(\vec{p})$	$a\Delta E'(\vec{p})$
0.8	2	5-20	0.6	0.060(2)	0.37(7)
1.0	2	5-20	0.5	0.051(2)	0.33(6)
1.2	2	5-20	0.4	0.045(2)	0.30(5)
1.7	2	5-20	0.2	0.034(2)	0.26(5)
2.0	2	5-20	0.2	0.029(2)	0.25(5)
2.5	1	13-20	0.2	0.025(2)	-
3.0	1	13-20	0.2	0.021(2)	-
3.5	1	13-20	0.1	0.019(2)	-
4.0	1	13-20	0.1	0.016(2)	-

Table 9: Fit parameters and values of $\Delta E(\vec{p})$ extracted from performing a simultaneous correlated fit to the ratios $C_{1l}(|\vec{p}| = 1)/C_{1l}(|\vec{p}| = 0)$ and $C_{2l}(|\vec{p}| = 1)/C_{2l}(|\vec{p}| = 0)$ for $\kappa_l = 0.1585$.

mass from both momenta is found to be less than one standard deviation for $aM_0 > 1.2$, and confirms the dispersion relation in equation 23. For the lighter meson masses the disagreement is less than 2σ but indicates the increase in significance of the $|\vec{p}|^4/8M_3^3$ contribution and $M_2 \neq M_3$. Hence, we take M_2 obtained from the lower value of momentum as more reliable. However, for meson masses around the B meson and less the statistical uncertainty in M_2 is becoming prohibitively high.

2. Perturbatively. Since the inequality of M_1 and M_2 is due to the omission of the constant term in the NRQCD action, Lorentz invariance can be restored by a shift to the heavy quark mass,

$$M_2 - M_1 = Z_m M_0 - E_0. \quad (24)$$

The mass renormalisation, Z_m , energy of a heavy quark in NRQCD, E_0 , and the corresponding mass shifts, $\Delta_{pert} = M_2 - M_1$, as calculated in perturbation theory are shown in table 11 [7]. The characteristic scales, $q_{Z_m}^*$ and $q_{E_0}^*$, of Z_m and E_0 respectively are also given and these indicate the reliability of the perturbative result; if the characteristic scale is very soft perturbation theory is not a reliable method of calculating the quantity. For aM_0 around 2.0 and $aM_0 = 7.0$ and 10.0 the characteristic scales are hard and perturbation theory works well. However, as $aM_0 \rightarrow 5$, $q_{Z_m}^*$ becomes softer. This defect is due to the method of calculating the characteristic scale and does not relate to any physical effect. We use the suggestion of Morningstar [7] to guess a characteristic scale \bar{q} to smooth over the defect. The result Δ_{pert}^\dagger is also shown in the table. We also used this method of

aM_0	$aM_2(\vec{p} = 1)$	$aM_2(\vec{p} = \sqrt{2})$
0.8	1.25(5)	1.16(4)
1.0	1.49(6)	1.40(4)
1.2	1.69(8)	1.61(6)
1.7	2.25(14)	2.20(10)
2.0	2.64(20)	2.63(20)
2.5	3.07(27)	3.19(29)
3.0	3.66(39)	3.74(41)
3.5	4.05(48)	4.27(53)
4.0	4.81(79)	4.96(69)

Table 10: M_2 obtained from $a|\vec{p}| = 1$ and $a|\vec{p}| = \sqrt{2}$ for $\kappa_l = 0.1585$.

estimating the perturbative result for the lighter heavy quark masses where q^* is soft because NRQCD breaks down.

The mass shift is also shown in table 12 along with an error estimating the higher loop corrections omitted in this calculation. The uncertainty associated with E_0 is computed as detailed in section 5.2. For the quantity $M_0 Z_m$ we estimate the two loop contributions to be roughly $(M_0(Z_m - 1))^2$; this is a more conservative choice than the naive estimate of $M_0(Z_m - 1)^2$.

- From the dispersion relation of the heavy-heavy meson at the same M_0 . As mentioned above $M_2 - M_1$ is due to a mass shift of the heavy quark and therefore the shift for a heavy-light meson should be half that for a heavy-heavy meson with the same bare heavy quark mass:

$$\Delta_{hh} = \frac{1}{2}[M_2(hh) - M_1(hh)] \quad (25)$$

We used the NRQCD action including all relativistic corrections to $O(Mv^4)$ and the same method of extracting M_2 . The results are shown in table 12. As mentioned in Section 2 discretisation errors in the heavy quark momentum become significant around $aM_0 \sim 5$ and thus the results for $aM_0 = 7.0$ and 10.0 are not reliable.

All three methods of computing the mass shift are compared in table 12. There is reasonable agreement for $aM_0 \leq 4.0$, while for the heavier quark masses agreement is not expected due to the large systematic errors associated with Δ_{hh} . The estimate of the perturbative result for $aM_0 = 0.8 - 1.2$ and 4.0 appears to work well. Furthermore, the agreement between obtaining the heavy-light meson mass directly and methods 2 and 3 which assume a mass shift can be applied to the heavy quark mass confirms that Lorentz invariance can be restored in this

aM_0	n	$aq_{Z_m}^*$	Z_m	$aq_{E_0}^*$	aE_0	$a\Delta_{pert}$	$a\Delta_{pert}^\dagger$
0.8	4	0.04	–	0.03	–	-	0.886
1.0	4	0.19	0.668	0.14	–	-	1.063
1.2	3	0.31	1.755	0.27	1.481	0.625	1.254
1.7	2	0.49	1.253	0.48	0.402	1.728	-
2.0	2	0.54	1.197	0.55	0.372	2.022	-
2.5	2	0.56	1.146	0.62	0.359	2.506	-
3.0	2	0.52	1.119	0.68	0.349	3.008	-
3.5	1	0.34	1.155	0.71	0.348	3.695	-
4.0	1	0.23	–	0.74	0.346	-	3.944
7.0	1	25.10	0.994	0.79	0.350	6.608	-
10.0	1	4.11	0.978	0.81	0.351	9.430	-

Table 11: Perturbative results for $M_2 - M_1$. Δ_{pert}^\dagger is obtained using $\alpha_V(q^*, \bar{q})$ [7], where $\bar{q} = 0.6$ and 0.8 , and the resulting two values for the mass shift are averaged. For $aM_0 = 0.8, 1.0$ and 4.0 , ‘–’ indicates α_S is ill-defined at the corresponding value of $q_{Z_m}^*$ or $q_{E_0}^*$.

way. Since using the heavy-heavy dispersion relation is the most accurate method we use Δ_{hh} for $aM_0 \leq 4.0$ and the perturbative results for the two heaviest quark masses. Using $a^{-1} = 1.8-2.4$ we find $aM_0 = 2.4-1.7$ corresponds to the bare b quark mass.

5.3 Mass Splittings

5.3.1 Hyperfine Splitting

We extracted the hyperfine splitting by performing a single exponential fit to the jackknife ratio of the 3S_1 and 1S_0 C_{1l} correlators. The effective mass for $aM_0 = 1.0$ and $\kappa_l = 0.1585$ is shown in figure 10 along with the hyperfine splitting extracted as t_{min} is varied. The plateau begins at $t_{min} \gtrsim 11$, and this is found to be the case for all aM_0 . The splittings extracted using a fitting range of $11 - 20$ are shown in table 4.

Figure 11 presents the hyperfine splitting as a function of $1/M_{PS}$, where M_{PS} is the 1S_0 meson mass. Performing correlated fits to $E_{sim}^V - E_{sim}^{PS}$ using a fit function of the form in equation 15 and the same fitting procedure we found linear dependence on $1/M_{PS}$ around the B meson and down to $aM_0 = 1.2$. The extrapolation to the static limit is consistent, within 2σ , with zero; the uncertainty in the meson mass has not been included in the fit. This is largest for the heaviest two points. If these are omitted the extrapolation to infinite heavy quark mass is closer to zero. The coefficients extracted were stable over

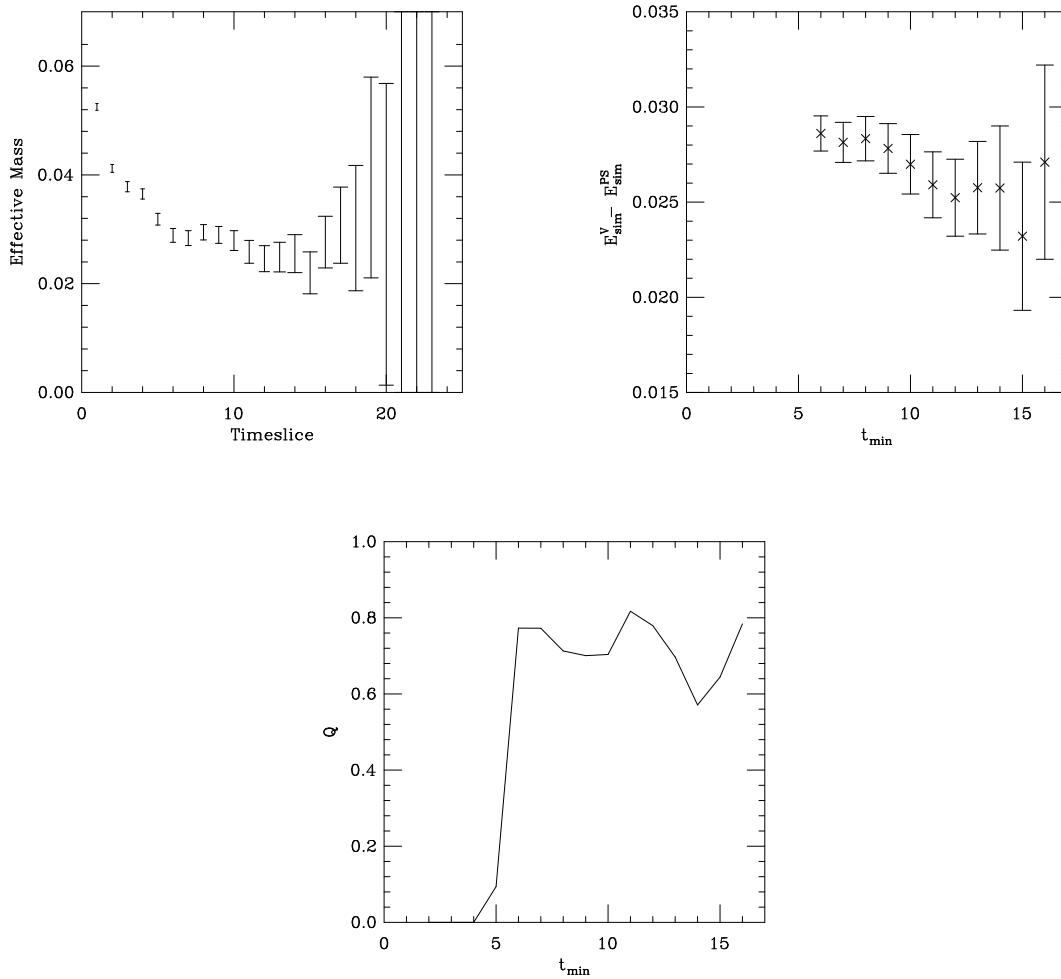


Figure 10: Shown are the effective mass of the ratio of 3S_1 to 1S_0 C_{1l} correlators for $aM_0 = 1.0$ and $\kappa_l = 0.1585$ and the mass splitting extracted using $n_{exp} = 1$ as a function of t_{min} . The corresponding values of Q are also shown. t_{max} is fixed at 20.

aM_0	$a\Delta_{hh}$	$a\Delta_{pert}$	$a\Delta_{hl}$
0.8	0.89(2)	0.89(34)	0.78(5)
1.0	1.09(3)	1.06(30)	1.00(6)
1.2	1.27(2)	1.25(31)	1.20(8)
1.7	1.76(2)	1.73(35)	1.74(14)
2.0	2.07(2)	2.02(30)	2.13(20)
2.5	2.58(2)	2.51(26)	2.56(27)
3.0	3.10(3)	3.01(25)	3.14(39)
3.5	3.64(3)	3.70(31)	3.53(48)
4.0	4.12(4)	3.94(20)	4.29(79)
7.0	8.10(10)	6.61(12)	-
10.0	13.80(25)	9.43(22)	-

Table 12: Heavy quark mass shifts determined from the heavy-light dispersion relation, Δ_{hl} , perturbation theory, Δ_{pert} and the heavy-heavy dispersion relation Δ_{hh} .

the fitting range and we find

$$aC_0 = 0.016(7) \quad a^2C_1 = 0.038(2). \quad (26)$$

where the coefficient of the slope corresponds to $\frac{a^2}{2} < c_B \sigma \cdot B >_{renorm}^{tadpole-improved}$. This is consistent with $O(a^2 \Lambda_{QCD}^2) \sim 0.04$ expected from naive power counting. In addition, agreement is found with our results on quenched configurations, $a^2C_1 = 0.043(6)$ [3]. Converting to physical units,

$$\langle c_B \sigma \cdot B \rangle_{renorm}^{tadpole-improved} = 0.24 - 0.44 \text{ GeV}^2 \quad \beta^{(n_f=2)} = 5.6 \quad (27)$$

$$= 0.362 \pm 50 \pm 36 \text{ GeV}^2 \quad \beta^{(n_f=0)} = 6.0 \quad (28)$$

where for the quenched results the first error is statistical and the second is due to the uncertainty in a^{-1} . This compares reasonably well with an explicit measurement of the naive matrix element obtained by Ewing et al [15] on quenched configurations using tree-level Clover fermions at $\kappa_l = \kappa_s$ and $\beta^{(n_f=0)} = 6.2$: $Z_\sigma < \sigma \cdot B > = 0.465 \pm \frac{25}{25}(\text{stat}) \pm \frac{65}{60}(\text{syst}) \text{ GeV}^2$, where Z_σ is the renormalisation factor required in the static theory.

We find no dependence of the splitting on the light quark mass, and this is also found in experiment: $B^* - B = 46(1) \text{ MeV}$ and $B_s^* - B_s = 47(3) \text{ MeV}$. We find a splitting of 25–40 MeV; the large uncertainty in the splitting reflects the particular sensitivity to the lattice spacing arising from the $1/M_{PS}$ dependence. While the hyperfine splitting is uncertain it does appear to lie below the experimental value. This may be due to residual quenching effects, the correct number

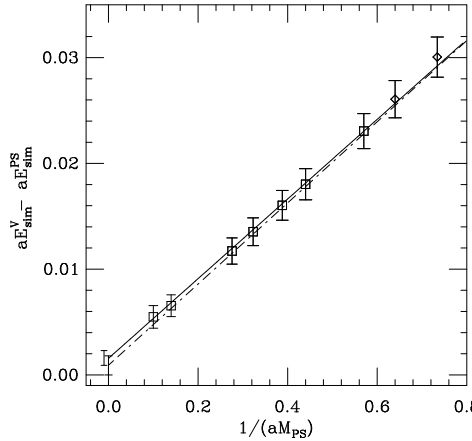


Figure 11: The hyperfine splitting vs $1/(aM_{PS})$ for $\kappa_l = 0.1585$. The solid line indicates a linear fit to the data shown as squares. The dashed line indicates a linear fit to the data (squares) omitting the heaviest two points.

of quark loops being $n_f \sim 3 - 4$. The splitting is proportional to the wavefunction at the origin and is dominated by a harder physical scale than those which characterise the quantities used to calculate the lattice spacing. Hence, it is a quantity which is sensitive to quenching effects.

5.3.2 P-S Splitting

The first measurements of the P-states of the B mesons have recently been made at DELPHI and OPAL [16, 17]. This provides a further test of the lattice simulation of B mesons through comparison with experiment, and also a ideal quantity with which to extract a value for the lattice spacing from the B system itself; the $P - S$ splitting is expected to be very weakly dependent on the heavy quark mass. So far the spin splittings of the P-states have not been clearly resolved and the experiments above find $B^{**} - \bar{B} = 419(25)$ MeV, where a cross-section weighted mean is used for B^{**} . A more detailed discussion of the comparison of our quenched results to experiment is given in [3].

We obtain a signal for the 1P_1 , 3P_0 and 3P_1 correlators; the 3P_2 is too noisy to extract an estimate of the mass. However, the spin-splittings between the P-states are consistent with zero. This is shown in figure 12 which displays the effective masses of the 1P_1 C_{1l} and C_{11} correlators and the $^3P_1 - ^1P_1$ and $^3P_0 - ^1P_1$ splittings for $aM_0 = 1.0$ and $\kappa_l = 0.1585$. The spin-orbit interaction of the light quark, which we expect to split the $j_l = 3/2$ and $j_l = 1/2$ states by $50 - 100$ MeV [18], is below the level of our statistical errors. A multi-smearing analysis is not possible for the P-states, the first excited state smearing function used for the P states (see equation 7) had almost identical overlap with the ground and excited states as

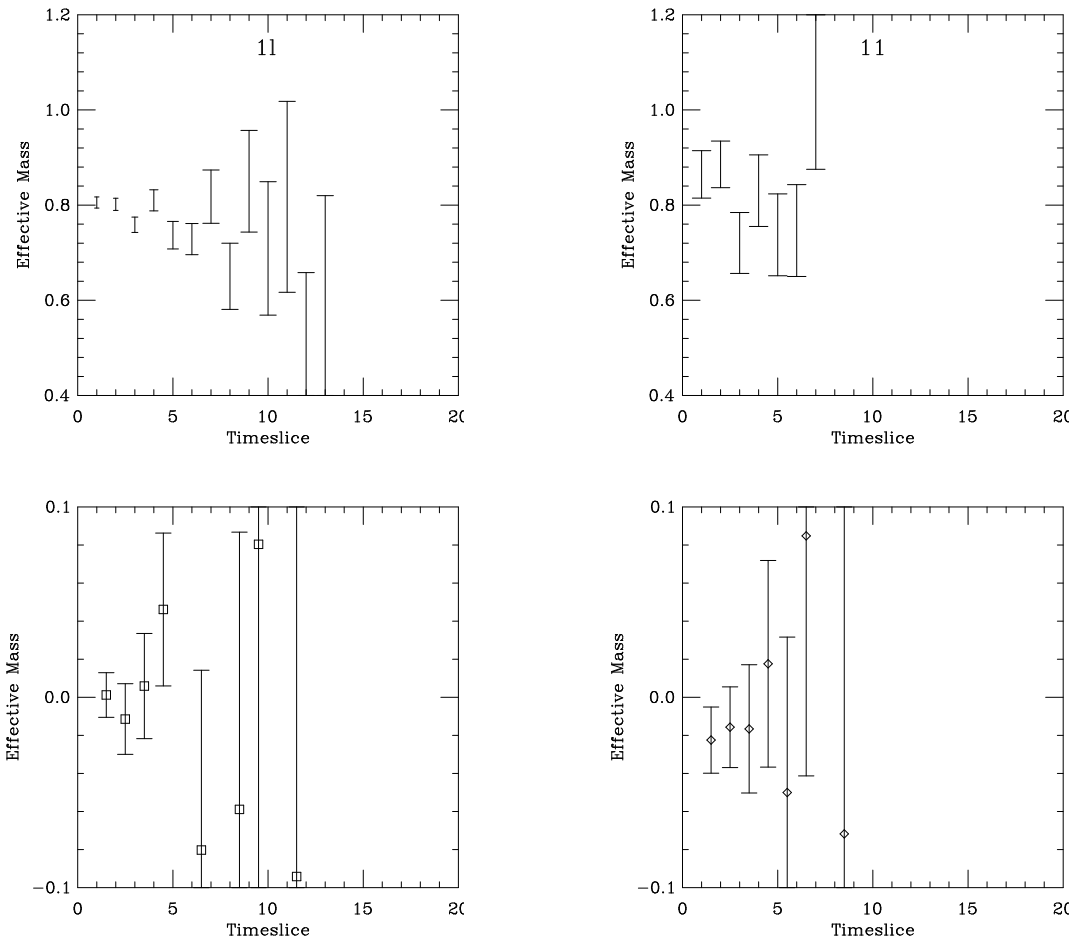


Figure 12: The effective masses of the ${}^1P_1 C_{1l}$ and C_{11} correlators, and the ratios of the 3P_1 and ${}^1P_1 C_{1l}$ correlators (squares), and 3P_0 and ${}^1P_1 C_{1l}$ correlators (diamonds).

the ground state smearing function.

As we are unable to resolve spin-splittings, we considered only the 1P_1 state and performed $n_{exp} = 1$ fits to C_{1l} and C_{11} separately. A simultaneous fit to both correlators was not possible since the C_{11} correlator becomes dominated by noise as C_{1l} plateaus. The results, given in figure 13, show a fairly significant discrepancy between the energies, stable in t_{min} , from the two fits. Unusually, the values from C_{11} lie above those for C_{1l} , which does not approach a plateau from below. Since noise dominates the ${}^1P_1 C_{11}$ correlator around $t \sim 10$ it is possible that this correlator has not plateaued and the results from the C_{1l} correlator, which can be checked over a larger range of t_{min} , are more reliable.

In order to investigate the dependence of the $P-S$ splitting on the heavy quark mass we calculated the splitting at $aM_0 = 1.0, 1.7$ and 4.0 . From table 13

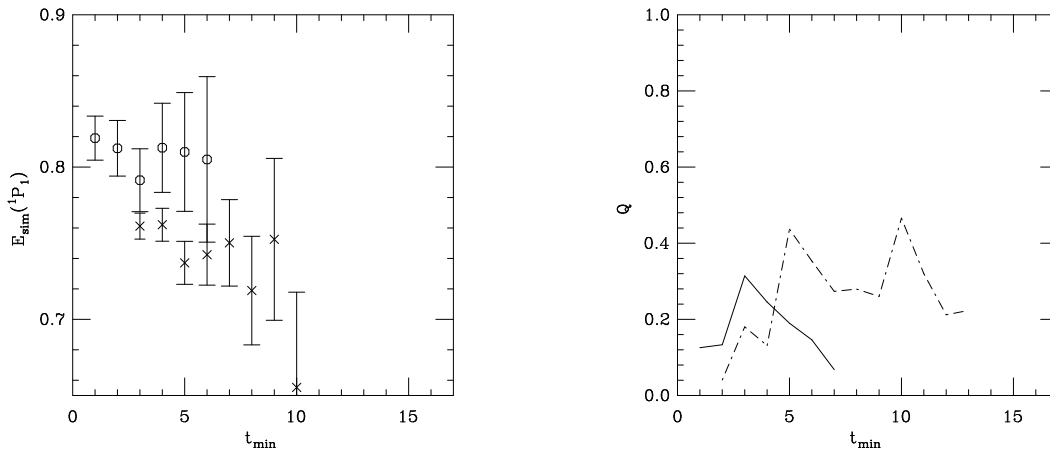


Figure 13: The 1P_1 energy extracted from a $n_{exp} = 1$ fit to C_{1l} (crosses) and C_{11} (circles) correlators separately and the corresponding values of Q (dashed and solid line for the fits to C_{1l} and C_{11} respectively) for $aM_0 = 1.0$ and $\kappa_l = 0.1585$. t_{max} is fixed to 12 for C_{1l} and 10 for C_{11} .

the $^1P_1 - \bar{S}$ splittings, where \bar{S} is the spin-averaged S-state, are $O(\Lambda_{QCD})$ as expected for the excitation of a light quark and only mildly dependent on the heavy quark mass. The results are plotted against $1/M_{PS}$ in figure 14. Considering the discrepancy of $\sim 3\sigma$ between the fits for C_{1l} and C_{11} the dependence on M_0 is not significant. We find no dependence of $^1P_1 - \bar{S}$ on the light quark mass and using $aM_0 = 1.7$ we obtain a splitting of 400–700 MeV. The characteristic scale for the $^1P_1 - \bar{S}$ splitting is expected to be similar to that for light spectroscopy. However, using the experimental result to determine the lattice spacing, $a^{-1} = 1.6(5)$ GeV, where the uncertainty due to fitting is included in the error. With such a large error this determination of the scale is not particularly useful and is consistent with all the other estimates of a^{-1} . An improvement in the smearing functions and a resolution of the spin-splittings both in the simulation and in experiment is needed in order to provide a useful determination of the lattice spacing.

5.3.3 $B_s - B_d$ Splitting

Another quantity of interest is the $B_s - B_d$ splitting, which is expected to be very weakly dependent on the heavy quark mass at the $O(m_s/M)$ level. In addition, as the splitting is the difference of the B_s and B_d binding energies it is expected to be $O(m_s) \sim 100-300$ MeV. Experimentally, $B_s - B_d = 98(6)$ MeV. In order to extract the splitting we chirally extrapolated E_{sim}^{PS} using the energies from the data at $\kappa_l = 0.1600$ which are extracted using the $n_{exp} = 1$ fits to C_{11} correlators with the fitting range 3–20. Figure 15 presents our results for the splitting, which are consistent with no heavy quark mass dependence. Converting

aM_0	C_{1l}	C_{11}	$a(^1P_1 - \bar{S})$
1.0	0.74(1)	0.81(2)	0.28(6)
1.7	0.74(1)	0.80(2)	0.26(5)
4.0	0.73(1)	0.80(2)	0.25(5)

Table 13: Energy of the 1P_1 state obtained from $n_{exp} = 1$ fits to C_{1l} using the fitting range 5 – 15 and C_{11} using 3 – 10 for $\kappa_l = 0.1585$. Also shown is the $^1P_1 - \bar{S}$ splitting, where the error bars take into account the uncertainty due to fitting.

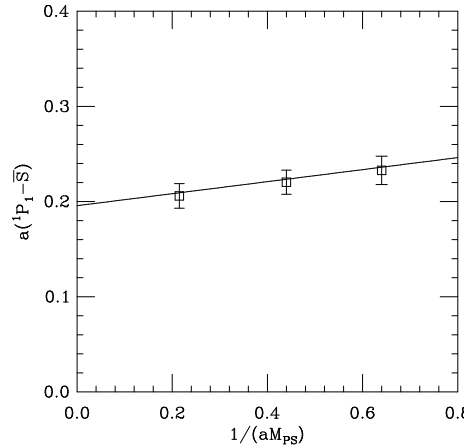


Figure 14: The $a(^1P_1 - \bar{S})$ splitting obtained using fits to the 1P_1 C_{1l} correlator vs $1/(aM_{PS})$ for $\kappa_l = 0.1585$.

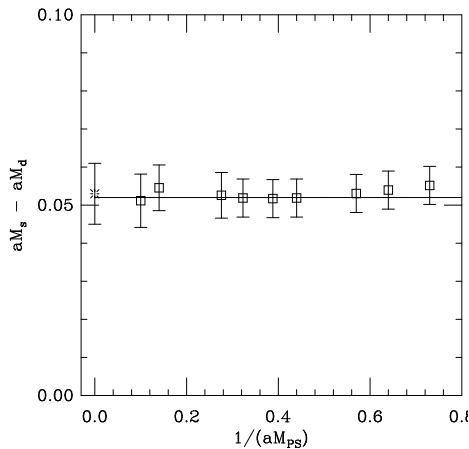


Figure 15: The $aM_s - aM_d$ splitting vs $1/(aM_{PS})$, where $\kappa_s = 0.1577$ is obtained using the ratio M_ϕ/M_ρ . The burst indicates the static result which is not included in the fit.

to physical units we obtain $B_s - B_d = 90 - 130$ MeV; consistent with experiment within the large systematic uncertainties arising from both κ_s and a^{-1} .

6 Conclusions

We presented a lattice study of the heavy-light spectrum in the region of the B meson, the first to partially include the effects of dynamical quarks. A multi-smearing, multi-state fitting analysis was performed and the ground S and P states as well as the excited S states were extracted. Figure 16 summarizes the results for the B spectrum. This is a high statistics calculation and the systematic errors arising from the Wilson light quarks, indicated in the figure, are the dominant uncertainty. Within these errors the results obtained are in agreement with experiment. We are in the process of repeating the calculation using tadpole-improved Clover light fermions. This will allow a comparison with our quenched results, in progress, which use the same light fermions.

We performed a comprehensive calculation of the heavy-light meson mass, investigating three methods and their range of validity. The agreement found between these methods confirms that Lorentz invariance can be restored at this order in NRQCD by a constant shift to all masses.

We calculated the spectrum over a wide range of heavy quark masses enabling a detailed investigation of heavy quark symmetry. For the binding energy and mass splittings the corrections to the heavy quark limit were found to be in agreement with naive expectations based on a hydrogen-like picture of the heavy-light meson. However, there is an indication from the mass dependence of the ground

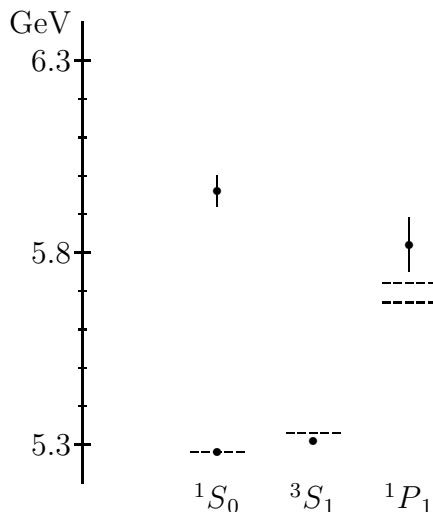


Figure 16: The B spectrum. The filled circles denote our results, where $a^{-1} = 2.0$ GeV has been used to convert to physical units and the error bars do not take into account uncertainties in a^{-1} . The open circle indicates the estimate of the systematic uncertainty in the $2S - 1S$ and $1P_1 - S$ splitting. The dashed lines denote the upper and lower bounds on the experimental results. The B mass has been shifted upwards to match the physical value.

S -state energy that for quark masses around M_b the next order in the NRQCD expansion is required. Using our tadpole-improved approach the nonperturbative coefficients $\bar{\Lambda}$ and $\langle -\bar{D}^2 \rangle$ were extracted. We showed that previous lattice calculations have large tadpole contributions and when we correct for this using mean field theory we find agreement with our results. The major error remaining is a perturbative one.

7 Acknowledgements

The heavy-light computations were performed on the CM-2 at SCRI. The heavy-heavy simulations used in section 5.2.1 were performed on the CRAY-YMP at the Ohio Supercomputer Center. We thank the HEMCGC collaboration for use of their configurations and light quark propagators. We are grateful to C. Morningstar and G. P. Lepage for useful discussions. J. Shigemitsu thanks the members of the lattice group at SCRI for their hospitality during a long term visit when part of this research was carried out. This work was supported by the U.S. DOE under grants DE-FG02-91ER40690, DE-FG05-85ER250000 and DE-FG05-92ER40742, and the UK PPARC and SHEFC. We acknowledge support by

NATO under grant CRG 941259 and the EU under contract CHRX-CT92-0051.

References

- [1] C. T. H. Davies et al, Phys. Rev. **D50** 6963 (1994).
- [2] P. McCallum and J. Shigemitsu, talk presented at the *International Symposium on Lattice Field Theory, Melbourne, Australia, 11-15 July 1995*, to appear in Nucl. Phys. **B** (Proc. Suppl.), hep-lat-9510006.
- [3] A. Ali Khan et al, Glasgow preprint no: GUTPA/95/12/1, SCRI preprint no: FSU-SCRI-95-121, Ohio preprint no: OHSTPY-HEP-T-95-026, hep-lat-9512025. Submitted to Phys. Rev. **D**.
- [4] S. Collins et al, talk presented at the *International Symposium on Lattice Field Theory, Melbourne, Australia, 11-15 July 1995*, to appear in Nucl. Phys. **B** (Proc. Suppl.), hep-lat-9512027.
- [5] UKQCD Collaboration, in preparation.
- [6] K. M. Bitar et al, Phys. Rev. **D46** 2169 (1992).
- [7] C. J. Morningstar, Phys. Rev. **D48** 598 (1993) and private communication.
- [8] A. Duncan et al, Phys. Rev. **D51** 5101 (1995).
- [9] S. Hashimoto, Phys. Rev. **D50** 4639 (1994).
- [10] M. Crisafulli et al, Nucl. Phys. **B457** 594 (1995).
- [11] APE Collaboration, C. R. Allton et al, Nucl. Phys. **B413** 461 (1994).
- [12] A. Ali Khan and C. T. H. Davies, in preparation.
- [13] S. Collins et al, in preparation.
- [14] T. Onogi and J. N. Simone, Nucl. Phys. **B** (Proc. Suppl.) **42** 434 (1995).
- [15] UKQCD Collaboration, A. K. Ewing et al, Edinburgh preprint no: 95/550, Southampton preprint no: SHEP 95-20, Swansea preprint no: SWAT/78, hep-lat-9508030.
- [16] DELPHI Collaboration, Phys. Lett. **B345** 598 (1995).
- [17] OPAL Collaboration, Z. Physik **C66** 19 (1995).
- [18] J. L. Rosner, Comm. Nucl. Part. Phys. **16** 109 (1986).